Generating Oscillatory Behavior by Applying a Magnetic Field during Electrocatalytic Oxidation of Glycerol

Rui Gao, Mohamad S. Kodaimati, Kaitlyn M. Handy, Samuel E. Root, and George M. Whitesides*

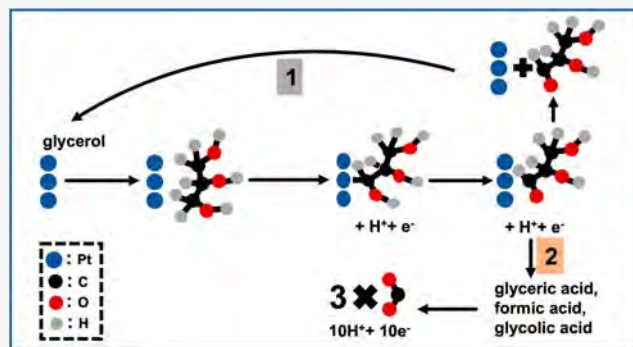Cite This: *J. Phys. Chem. C* 2022, 126, 18159−18169

Read Online

ACCESS | Metrics & More | Article Recommendations | SI Supporting Information

ABSTRACT: This work demonstrates how the application of a magnetic field during electrocatalysis can affect the transport of reactants and products at the electrode surface and, under certain conditions, generate complex, oscillatory behavior in amperometric experiments. During the electrocatalytic oxidation of glycerol (EOG), the Lorentz force acts upon hydronium and hydroxide ionic currents to produce fluidic convection, which serves to enhance the mass transport of glycerol and glyceraldehyde. Particle imaging velocimetry shows that the convective fluid flow field depends nonlinearly on the viscosity of the solution (dictated by the concentration of glycerol, which ranged from 2.5% to 40% v/v, to give a viscosity range of 1.3−5.3 mPa s). The nonlinear dependence of velocity of the fluid flow on the viscosity of the electrolyte generates time-delayed negative feedback during EOG and results in chemical oscillations. This time-delayed feedback is due to two coupled steps: (i) oxidation of glycerol rapidly decreases the viscosity of the electrolyte near the anode and (ii) at low viscosities magnetic fields increase the rate of mass transport, which subsequently increases the viscosity of the electrolyte near the anode (by increasing the concentration of glycerol). These chemical oscillations can be used to enhance the selectivity of EOG to glyceric acid by a factor of 2.1. This work focuses on the effects of magnetic fields on EOG using a combination of fluid flow analysis, rotating-disk electrode experiments, and electrochemical simulations.
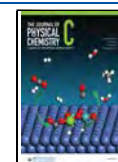
■ INTRODUCTION

With the goal of producing new molecules/products, synthetic chemistry has generated reactions mechanism that are increasingly complex,[1,2] that is, involving the interaction of multiple chemical species and/or reactions.[3−6] One example of a complex chemical system is the tandem catalysis used by Yang and co-workers to hydrogenate CO_2 to C_2−C_4 hydrocarbons using a nanostructured CeO_2−Pt catalyst coated with a mesoporous SiO_2−CO interface.[7] Synthetic chemistry is still unable to duplicate the complexity found in biochemical reactions; synthetic chemistry relies upon careful control of the initial reaction conditions (e.g., concentrations, temperature, pressure, etc.) to reach the desired products/outcomes. As a reaction progresses, these reaction conditions can change— requiring *external* intervention to maintain these conditions (i.e., using an ice bath when reducing an ester with $LiAlH_4$). This external intervention occurs on much longer time scales (<10 s^{-1})[8] than chemical processes (10^2−10^6 s^{-1} for proton reduction using transition-metal molecular catalysts)[9−13] and is unable to respond effectively to rapid changes in the chemical system. Biological systems can operate with no external intervention and can rapidly respond to changes in the environment. These biological reactions are dynamically regulated by signaling pathways. For example, neuronal cells must regulate intracellular and extracellular concentrations of

K^+ to maintain the membrane potential necessary for neurotransmission.[14] Dynamic regulation can potentially enable synthetic catalysts to access new kinetic products and product distributions and enhance overall catalytic activity and robustness.[15−18] In this work, we design a complex electrochemical system by applying a magnetic field during electrocatalytic oxidation of glycerol (EOG). We refer to a chemical system as complex if it displays emergent or nonadditive behavior (different than the sum of its parts).[15,17−19] Complex chemical systems are generally sensitive to initial conditions/small perturbations and can evolve down multiple pathways.[19,20] Complex chemical systems couple multiple *chemical* reactions and operate under one of two mass-transport conditions: (i) diffusion-limited transport[21,22] or (ii) near-perfect mixing (as in the continuous stirred-tank reactor, CSTR).[23−25] In this work, we couple the fluidic convection
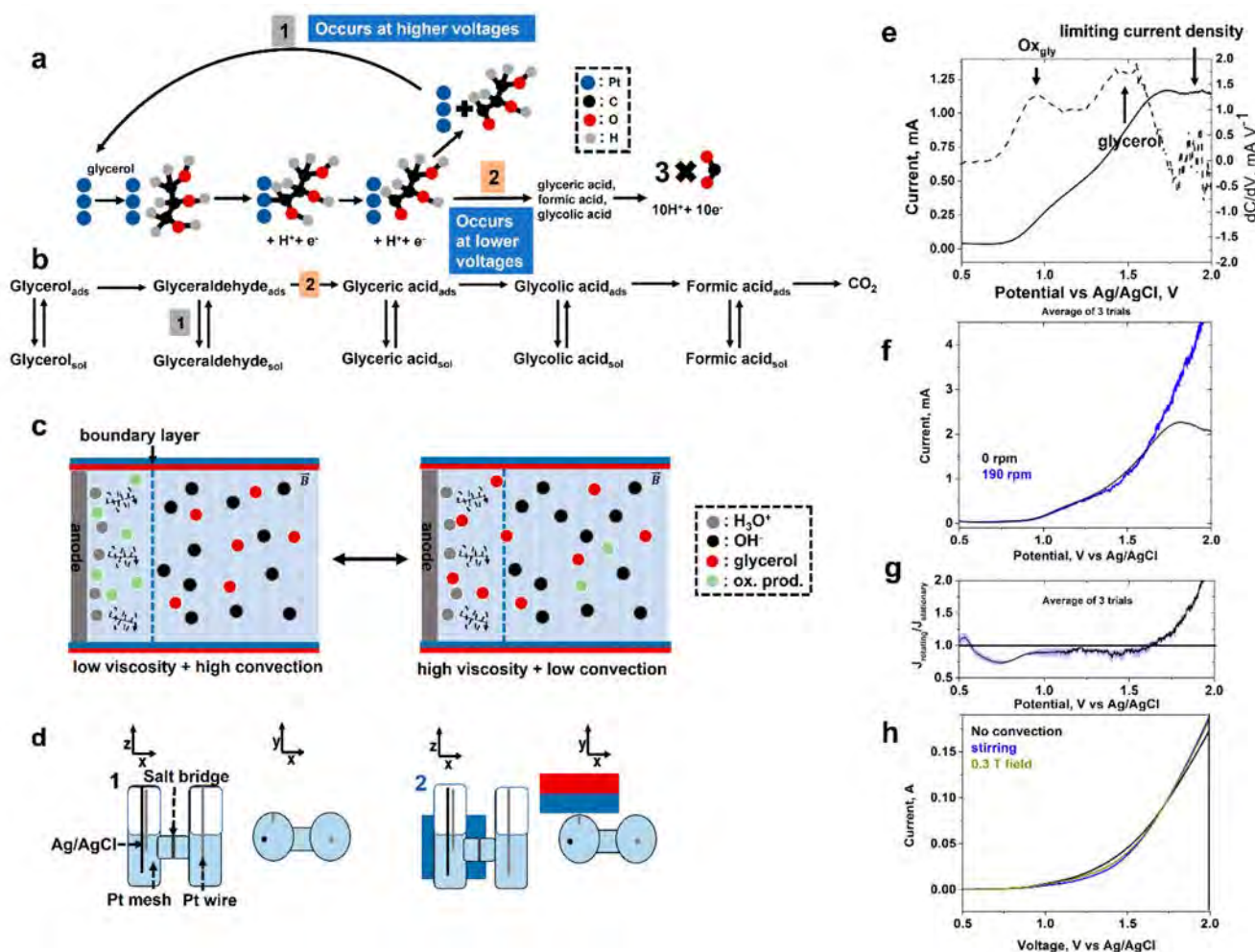
Figure 1. Schematic representation of our setup for generating complex behavior during the electrochemical oxidation of glycerol. (a) Schematic depiction of the oxidation of glycerol to glyceraldehyde, glyceric acid, formic acid, glycolic acid, and CO_2. Pathway 1 corresponds to dissociation of the adsorbed glyceraldehyde and continued oxidation of glycerol, and pathway 2 corresponds to continued electrocatalytic oxidation of glyceraldehyde. (b) Schematic showing the kinetic processes associated with dissociation of glyceraldehyde. (c) Schematic depiction of how this work uses magnetic fields to generate electrochemical oscillations. At low viscosities, the Lorentz force allows for more convection and increased mixing of the solution. The increased convection leads to an increase in the viscosity of the solution which decreases the current density. (d) Schematic representation of the electrochemical cell used to measure the effect of magnetic fields on oxidation of glycerol. (e) Plot of applied potential vs current (solid) and the derivative of the current with respect to the voltage (dashed) for a 25% v/v solution of glycerol in 1 M KOH. We indicate the two peaks corresponding to glycerol oxidation and glyceraldehyde oxidation. (f) Linear-sweep voltammograms showing the current density with a RDE at 0 rpm (black) and 190 rpm (blue) for a 10% v/v solution of glycerol in 1 M KOH. These results were averaged over three independent experiments. (g) Plot of the ratio of the current while rotating the electrode to the current when the disk is stationary to highlight the different catalytic regimes. The blue lines and shaded area correspond to the standard deviation of the three trials. (h) Linear-sweep voltammograms for a solution of 5% v/v glycerol in 1 M KOH with a Pt mesh electrode with no convection, stirring with a magnetic stir bar, and a 0.3 T field.

generated by magnetic fields to the electrocatalytic oxidation of glycerol and generate oscillatory behavior.

Glycerol is a byproduct in the production of biofuels—accounting for 7−10% (w/w) of the products—with >1 billion tons produced annually.[26−28] One potential commercial utilization of glycerol is as a fuel in direct alcohol fuel cells.[29−31] Glycerol has a high energy density (6.26 kWh L^{-1}),[32] is nontoxic, and has a high flash point (176 °C) and low vapor pressure (1.68×10^{-4} mmHg at 25 °C).[33] In a glycerol fuel cell, oxidation of glycerol to oxidized species (such as CO_2) and protons (electrocatalytic oxidation of glycerol, EOG) at the anode is coupled to the oxygen reduction reaction at the cathode (Figure 1a,b).[29,31,32] Kenis and co-workers recently demonstrated the potential techno-economic utility of coupling EOG to electrocatalytic reduction of CO_2.[34−36] EOG is typically done under alkaline or acidic conditions (to accelerate the reaction kinetics) with noble metal (Pt, Au, or Pd based) catalysts.[30,34,35] The kinetics and selectivity of EOG are highly sensitive to catalytic conditions including the glycerol concentration, the pH of the electrolyte, applied potential, and hydrodynamics of the electrochemical cell.[37−46] One obstacle in developing glycerol-based fuel cells is the lack of electrocatalysts with high selectivity for specific products for glycerol oxidation such as dihydroxyacetone, glyceric acid, and tartronic acid.[43] Polycrystalline Pt generally produces a mixture of oxidized two- and three-carbon products like oxalic acid, glyceric acid, and dihydroxyacetone, in addition to CO_2.[47−50] One obstacle to achieving high selectivities for EOG is that

more oxidized species (e.g., glyceric acid) formed during EOG typically desorb from the catalytic surface and prevent complete oxidation of the species—despite the applied potential being greater than the potential needed for that oxidative reaction (e.g., oxidation of glyceric acid).[42,44,47]

In this work, we demonstrate how magnetic fields can be used to generate oscillations in the electrochemical current (a complex behavior) during the EOG—specifically, we examine how the fluidic convection arising from the Lorentz force can be used to generate electrochemical oscillations by alternating between two catalytic pathways during EOG (Figure 1c,d). We[51] and others[52−55] have shown that magnetic fields can be used to increase mass transport in electrochemical systems through magnetohydrodynamic effects (MHD)[51,52,55,56] or magnetic fields interacting with paramagnetic species (e.g., Kelvin force/magnetic field gradient force).[53,54,57,58] The Lorentz force acting upon ions moving in the solution (discussed in more detail below) generates fluidic convection that enhances mass transport and modifies the observed reactivity.[51] The flow induced by a magnetic field can also interact with natural convective flow, caused by differences in local density (i.e., buoyancy), and/or paramagnetic ions, to produce electrochemical oscillations. Such complex electrochemical behavior has been observed during water electrolysis, where the magnetic field influences the detachment and subsequent trajectory of bubbles formed at the electrode surface, increasing the effectiveness of hydrolysis.[56] Additionally, electrochemical oscillations have been observed during the dissolution of iron ions[57] and the deposition of copper ions[58] in the presence of a magnetic field, where the oscillations were attributed to a mechanism by which the magnetic gradient, Lorentz force, and buoyancy force counteract one another.

The magnitude of the flow induced by the Lorentz effect is more pronounced for electrolytes of lower viscosity and systems with higher electrochemical current density.[52−55,59,60] Here, we exploit these dependencies to create electrochemical oscillations in EOG. We demonstrate, through a combination of experiments and simulations, a mechanism by which electrochemical oscillations are produced through the application of a magnetic field to a reaction in which the viscosity of the products are different than the reactants, and characterize the parametric regimes over which this phenomenon occurs.

■ METHODS

Electrode Preparation. We used a Pt mesh as the anode and Pt wire as the cathode. The Pt electrodes were >99.9% purity and obtained from MilliporeSigma. The wires were cleaned with Milli-Q water prior to use. The exposed geometric surface area of the Pt mesh was 6 mm × 12 mm.

Electrochemical Measurements. Electrochemistry experiments were performed using a CH Instruments Inc. electrochemical workstation. An Ag/AgCl (1 M KCl) electrode and a Pt wire were used as the reference and counter electrodes, respectively, in all measurements. Milli-Q water (18.2 MΩ·cm at 25 °C) was used in the preparation of all aqueous solutions. The electrodes were cleaned using by potentiometric stripping in 0.1 M H_2SO_4 prior to use. All materials were analytical grade (>99%, MilliporeSigma) and were used as supplied unless otherwise specified.

Gas Chromatography Analysis. We performed head-space gas chromatography (GC) experiments using an Agilent 6890A GC equipped with a Restek Shincarbon column (Agilent) and a thermal conductivity detector (TCD). To measure the amount of gas formed during bulk electrolysis experiments, we manually injected 100 μL of the sample headspace (5 mL total). We accounted for the partitioning of the gases in the liquid and gas-phases of the solution using Henry's law (see the Supporting Information for details).

Nuclear Magnetic Resonance. We performed nuclear magnetic resonance (NMR) experiments to quantify the concentrations of products formed in the liquid phase. We performed quantitative ^{13}C NMR on a 400 MHz Avance Neo NMR. We added gadolinium ethylenediaminetetraacetic acid as an NMR relaxation agent to aliquots of electrolysis experiments. Experiments were collected for 1024 scans with a 1 s relaxation delay (T_1) (see the Supporting Information for details).

Particle-Imaging Velocimetry Experiments. To analyze the fluid flow near the electrode surface, we used particle-imaging velocimetry (PIV) with 3 μm diameter fluorescent polystyrene microspheres in aqueous solutions composed of 1 M KOH and glycerol.[51,62] We performed the experiments using a Mightex SME-C050-U CMOS camera with a OPTEM 125× variable zoom lens. We used a 1280 × 1024 pixel exposure area with 4 pixel binning operating at 100 frames per second (fps). The electrochemical cell was diffusely illuminated using UV led lamps and fluorescent UV lamps. We analyzed the data by comparing the positions of particles between two successive frames and averaging over 5000 frames to obtain the velocity fields using PIVlab in MATLAB.[63] We numerically calculated the curl of the velocity fields in MATLAB to determine the vorticity of the fluid flow near the electrode—a useful measure of turbulent flow in fluids.[64]

■ RESULTS AND DISCUSSION

This paper focuses on demonstrating how the mass transport generated by the Lorentz force acting on electrochemical systems can be used to generate complex behavior in electrochemical systems; specifically, we show that application of a static magnetic field during electrocatalytic oxidation of glycerol can generate complex behavior. The reaction oscillates by switching between two primary reaction pathways: (1) oxidation of glycerol to glyceraldehyde and (2) oxidation of glyceraldehyde (and subsequently oxidized products) to species containing smaller numbers of carbon atoms (Figure 1). We use *static* magnetic fields to make electrochemical systems oscillate between these two pathways; these oscillations rely on the nonlinear relationships between the (i) viscosity of the solution, (ii) current density, and (iii) MHD effects.

Ionic currents are generated in EOG due to the (i) production of protons at the anode and consumption of protons at the cathode and (ii) electrophoretic transport of products away from the surfaces of the electrodes and reactants toward the surfaces of the electrodes (Figure 1). The net ionic current in the electrochemical cell involves negative ions (hydroxide ions) moving toward the anode and positive ions (hydronium ions) moving toward the cathode. When a static magnetic field, $\vec{B}$ [T], with components perpendicular to the ionic current is applied, the instantaneous force, $\vec{F}(t)$ [N], felt by an ion with charge, q [C], moving with instantaneous velocity $\vec{v}(t)$ [m/s] can be expressed using the generalized Langevin form of the Lorentz force, following eq 1

$$\vec{F}(t) = q(\vec{E} + \vec{v}(t) \times \vec{B}) - \int_0^t \gamma(t - t')\nu(t')\, \mathrm{d}t' + \xi(t)$$

(1)

where $\int_0^t \gamma(t - t')\nu(t')\, \mathrm{d}t'$ represents the drag on the ion and is obtained from a memory kernel integral of the dynamic friction coefficient, $\gamma(t)$.[61] The term $\xi(t)$ (in eq 1) is a stochastic force that represents Brownian-force-like collisions with solvent molecules. Equation 1 predicts that a charged particle in solution experiences a force in the direction of $\vec{E}$, a force orthogonal to the velocity of the particle and to $\vec{B}$ (following the right-hand rule), and field-independent drag and stochastic forces resulting from collisions with solvent molecules.[61] These frictional interactions mediate the translation of the Lorentz force acting on the ions into hydrodynamic flow within the fluid at the electrode surface.[52]

In our reaction scheme, low viscosities are characterized by high concentrations of products resulting from the oxidation of glycerol (Ox_{gly}) near the surface of the electrode. We group these oxidation products together as they are formed from the *in situ* oxidation of glycerol during the electrocatalysis, whereas the direct oxidation of glycerol occurs when glycerol is adsorbed to the surface of the electrode. The Lorentz force generates more convection than when there is no applied *B*-field, thus decreasing the concentration of Ox_{gly} near the surface of the electrode and increasing the concentration of glycerol near the surface of the electrode. As a result, the increased convection leads to an increase in the viscosity of the solution, and this increase in viscosity decreases the current density. Afterward, the increased viscosity and decreased current density decrease the strength of MHD-driven convection and led to oxidation of glycerol to Ox_{gly}. This oxidation continues until the viscosity near the electrode decreases (due to preferential oxidation of glycerol relative to Ox_{gly}) and restarts the cycle (Figure 1c). In summary, we propose that static magnetic fields can generate time-delayed feedback that allows for oscillation between the oxidation of glycerol and oxidation of Ox_{gly}. This oscillatory behavior occurs as the electrochemical switches between two states (a low-viscosity state and a high-viscosity state) that depend upon the partitioning of the glyceraldehyde between the surface of the electrode and the bulk of the solution.

Rotating-Disk Electrode Experiments. To explore the effect of a magnetic field ($\vec{B}$ field) on EOG, we performed electrolysis with a Pt wire cathode and a Pt mesh anode (6 mm × 12 mm) in an electrochemical H cell: (i) with no $\vec{B}$ field and (ii) with a $\vec{B}$ field oriented perpendicular to the Pt mesh (Figure 1d). The Supporting Information contains the specific details of our experimental procedure. We applied a $\vec{B}$ field by placing a 50.8 × 50.8 × 25.4 mm^3 (2 × 2 × 1 in.^{3} manufacturer specification) NdFeB magnet (N52 grade) perpendicular to the surface of the Pt mesh (Figure 1d). We use the following *xyz* coordinate space to describe the reference frame of our experiments: the *x* coordinate is perpendicular to and the *y* and *z* coordinates are parallel to the plane of the Pt mesh. The *y* component of the $\vec{B}$ field is ~0.3 T (measured using a gaussmeter, model GM-1-ST, AlphaLab Inc.) at the surface of the Pt mesh (with the *x* and *z* components ~0 T). In our experiments, the edge of the Pt mesh was located ~5 mm away from the surface of the magnet, and the width of the Pt mesh was 6 mm to generate an average magnetic field strength of 0.3 T (Figure S1). We used aqueous solutions of 1.0 M KOH (which served two functions: (i) to increase the pH of the

solution and (ii) as a supporting electrolyte) and a Ag/AgCl reference electrode. Experiments were performed in air unless performing product analysis; when measuring the products formed during EOG, we sparged the samples with Ar to measure accurately the gaseous species that were evolved during the reaction by gas chromatography (GC). At the cathode, we only observed the hydrogen evolution reaction (HER), whereas at the anode, we observed EOG. We focus on the effects of a $\vec{B}$ field on the anodic reactions unless otherwise noted.

When we performed a linear sweep voltammogram (LSV) on the electrochemical cell with Pt disk electrode as the working electrode, we identified three distinct voltage regimes: (i) the transport-limited current density regime, (ii) current associated with glycerol oxidation, and (iii) current associated with the oxidation of Ox_{gly} (Figure 1e). The dashed curve in Figure 1e corresponds to the derivative calculated from the voltammogram and highlights the three voltage regimes associated with oxidation of glycerol. The linear-sweep voltammogram (LSV) was collected after five LSV scans after ensuring that the sequential scans had minimal run-to-run variation. While Pt can also oxidize hydroxide ions at potentials greater than 1.2 V vs Ag/AgCl in KOH, we exclude Pt oxidation of hydroxide ions from this work (as it contributes <20% of the current) and has a featureless linear-sweep voltammogram (Figure S13). We also previously demonstrated that magnetic fields and changes in mass transport do not affect oxidation of hydroxide ions by Pt.[51]

We determined the primary products corresponding to each current regime by analyzing the products formed during electrolysis for 1 h with ^{1}H NMR and gas chromatography (GC) (see Table S1). Our product analyses and current density regimes are in agreement with previous reports of glycerol oxidation on polycrystalline Pt.[30,39,40,48] To determine the relationship between the current density in each regime, we performed experiments with a Pt rotating disk electrode (RDE)[41] and observed that increased mass transport decreased the current density associated with oxidation of Ox_{gly} and increased the current density associated with oxidation of glycerol and the transport-limited current density (Figure 1f,g). These results were consistent across individual experiments, and we plotted the average of three independent experiments in Figure 1f,g. We believe the noise is due to a combination of the formation of CO_2 bubbles during electrolysis that modified that electrochemical surface area and/or electrical interference from the motor of the RDE. Notably, we did not observe any evidence of potentiostatic oscillations with the RDE.

After carrying out the experiments with the RDE, we used a Pt mesh electrode to increase the surface area of the electrode and eliminate any ferromagnetic components from the system. For the Pt mesh electrode, we observed similar trends in the current densities upon application of a magnetic field to a Pt mesh where application of a magnetic field decreased the current associated with oxidation of Ox_{gly} and increased the current density associated with oxidation of glycerol (Figure 1g). We stirred the anodic compartment of the H cell while using a Pt mesh electrode; we observed the same trends as when we applied the magnetic field (Figure 1h)—an increase in the current corresponding to oxidation of glycerol and a decrease in the current corresponding to oxidation of Ox_{gly}. These results support our hypothesis that the magnetic fields increase the current density via an increase in mass transport.
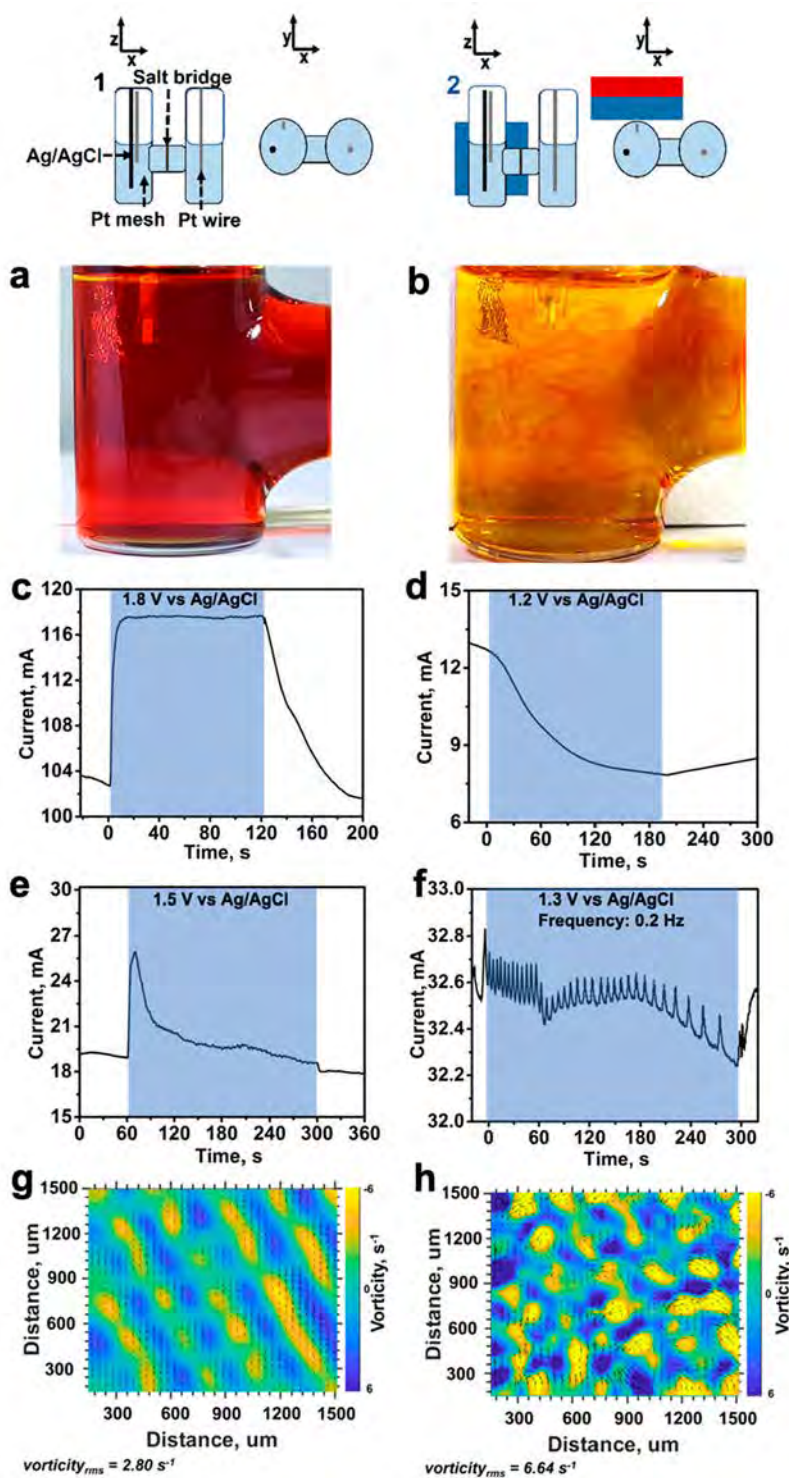
Figure 2. Pictures of solutions of 10% v/v glycerol in 1 M KOH with Alizarine as a pH indicator with no applied magnetic field (a) and a 0.3 T field (b). Plots of current vs time for four situations corresponding the four kinds of magnetic field responses that we identified of solutions of 10% v/v glycerol in 1 M KOH: a static increase in the current (c), a decrease in the current (d), overshooting (e), and oscillations (f). Blue regions correspond to time periods where we applied a 0.3 T field to the Pt mesh. Particle imaging velocimetry maps of the surface of the Pt mesh showing the velocity field (arrows) and vorticity (color map) for no magnetic field (g) and 0.3 T field (h). Stronger orange and blue regions correspond to regions of higher absolute values for the vorticity.

Observed Magnetic Field Effects. To confirm these effects, we performed electrochemical experiments with alizarine as a pH indicator. When we applied no magnetic field and no mechanical agitation (*e.g.*, stirring), we observed a uniform solution pH (Figure 2a and Video S1). When we applied a 0.3 T field, we observed the formation of helical currents in the solution and spatial heterogeneity of the solution pH (Figure 2b and Video S2).[51,52] We observed that magnetic fields increased nonuniformity of the pH of the solution (visualized using the pH indicator) and generated

The Journal of Physical Chemistry C

pubs.acs.org/JPCC

and glycerol concentration. The magnitude of the oscillations ranged from ∼0.2% of the current density (Figure 3b) to up to 24% of the current density (Figure S5). The periodicity of the oscillations ranged from ∼5 s (Figure S6) to ∼180 s (Figure 3c); the systems sustained oscillations for over 15 min (Figure 3c). We also observed that the system would be unable to sustain an oscillation or exhibited chaotic behavior (Figure S7).

To identify the mechanism through which oscillatory behavior developed, we analyzed the ratio of the current density of the magnetic field in the presence of a magnetic field (j) to the current density in the absence of a magnetic field (j_0), which we termed j/j_0. In this work, j/j_0 represents the enhancement in the current density due to the applied magnetic field. In the case of applying a magnetic field at a high potential (1.5 V vs Ag/AgCl), we observed that j/j_0 increased from ∼1.04 to ∼1.09 when the strength of the applied field was increased from ∼0.1 to ∼0.3 T (Figure 3d).

To confirm that the magnetic field effects arise due to mass transport, we consider how magnetic fields increase the rate of fluid flow using particle-imaging velocimetry (see the Supporting Information for details of the experiments and analysis). Briefly, we added 3 μm fluorescent particles while performing electrolysis to determine the fluid flow near the Pt mesh. When we compared the velocity field of the fluid and the magnetic field strength for a fixed concentration of glycerol (10% v/v), we observed that the velocity of the field increased as a function of the applied field strength, supporting the hypothesis that the magnetic field effects are due to an increase in mass transport (Figure 4a). If we assume that our system can be approximated as a 1-dimensional laminar flow system, the application of a 0.3 T magnetic field increases the mass transport by approximately a factor of 3.3 due to increase in the linear fluid velocity by a factor of 3.3 (Figure 4a). We consistently observed that in all cases the magnetic fields increased the velocity of the fluid from ∼2.5 to ∼8.3 mm s^{-1} near the surface of the electrode; this result contrasts with our electrochemical measurements (Figures 1 and 2), where we observed that the magnetic fields can increase or decrease the current density. These experiments parallel the results we obtained using a Pt RDE (Figure 1d). When we compared the effect of a magnetic field on the fluid velocity as a function of viscosity (modified by changing the concentration of glycerol), we observed that the magnetic fields always increased the fluid velocity relative to the case with no applied field (Figure 4b).

We ruled out possible Kelvin forces[54] on the electrochemical cell by performing experiments where we applied a magnetic field with either one magnet or two parallel magnets where opposite poles are facing each other (Figure S12). In the experiments with two magnets, the strength of the magnetic field is relatively uniform; by comparing the case of one magnet versus two magnets, we were able to measure the effect of the uniformity/gradient in magnetic field on the observed electrochemical current. We did not observe a significant difference between the two cases, which allowed us to rule out the effect of Kelvin forces in the system. Additionally, White and co-workers reported decreases in current and convection with specific orientations of the electrode due to the use of microelectrodes where the competition between the natural convection arising during the reaction and the convection generated by the magnetic fields could decrease the current.[54] In their reported cases, the decrease in current was due to a decrease in the convection near the surface (a destructive interference between natural convection and the convection

Figure 4. (a) Plot of RMS velocity of the fluid derived from particle-imaging velocimetry (PIV) vs the magnetic field strength. (b) Plot of RMS velocity of the fluid derived from particle-imaging velocimetry vs the viscosity of the solution in the presence of a 0.3 T magnetic field (black) and no applied field (blue). (c) Phase map highlighting the different regimes of magnetic field effects as a function of glycerol volume fraction and applied voltage. Blue regions correspond to the magnetic field increasing the current density. Red regions correspond to the magnetic field decreasing the current density, and green regions correspond to the magnetic field inducing oscillations in the current density.

generated by the magnetic fields). In cases where we observed that the magnetic fields increased the current or decreased the current, we observed that magnetic fields increase fluid flow (Videos S3 and S4, Figure 4), so we rule out the electrochemical oscillations being generated by the natural convection of the system.

Finally, to characterize the parametric regime over which this oscillatory system operates, we systematically varied the volume fraction of glycerol and the applied voltage during EOG while applying a 0.3 T field. We classified the behavior into three categories: (i) an increase in the current density, (ii) a decrease in the current density, or (iii) oscillatory behavior

Figure 5. (a) Simplified summary of the simulation used in this work. We used a 1D simulation where transport between cells was due to diffusion and convection. The convection time was inversely proportional to the current density. (b) Sample simulated electrochemical data showing that we can generate oscillatory behavior by adding convective process inversely proportional to the current density through the presence of the magnetic field.

(Figure 4c). We observed that as we increased the glycerol concentration, the voltages, for which oscillatory behavior is observed, increase in magnitude and broadened. We observed that the regions over which oscillations are finely delineated— a difference of 0.025 V can separate oscillatory versus linear behavior— and reproducible (samples were reproduced at least three times to be included in the data). We believe that one could also increase the size of the parameter space over which oscillations are observed by modifying other parameters that independently change the viscosity of the system (e.g., replacing the H_2O with D_2O). The density (1.1 g/cm^3) and viscosity (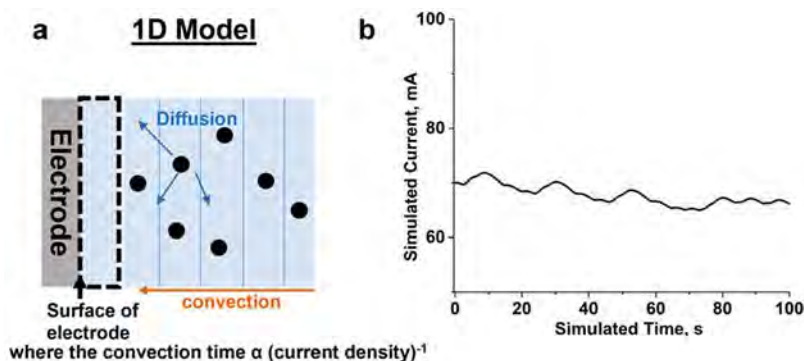1.25 mPa s) of D_2O are higher than those of H_2O (with a density of 1.0 g/cm^3 and viscosity of 1.0 mPa s) at 20 °C.[33] We would expect to see changes in the oscillation frequency, magnitude, and the parameter space over which we observed these oscillations. When we performed experiments using D_2O as the solvent (rather than Milli-Q H_2O), we observed the same qualitative trends as when we used H_2O as the solvent (Figure S10). We observed that the application of a magnetic field was able to increase the current (Figure S10a), decrease the current (Figure S10b), and generate unstable oscillations (Figure S10c). When we quantitatively compared the magnetic field effects on solutions with H_2O and D_2O (Figures 2 and S10), we observed that the solutions with D_2O had a smaller change in current density that solutions with H_2O—consistent with an increase in the density of the solution. We suspect this change in density is the primary source of disagreement between solutions composed of H_2O and D_2O, and further works can attempt to independently change the density of the solution (while keeping all other parameters the same) through the addition of polymers with differing molecular weights such as dextran and poly(ethylene glycol).

To help characterize this system, we performed kinetic simulations of the system to understand how the magnetic fields could influence the rate equations in the experimental system (see the Supporting Information for details concerning the kinetic simulations). Briefly, we performed kinetic simulations using a simplified model involving three species: (i) glycerol, (ii) glyceraldehyde, and (iii) Ox_{gly} (excluding glyceraldehyde). In our simulations, we simulated the effect the of the magnetic fields by adding a convective component to the transport of the chemical species where the convective transport time is inversely proportional to electrochemical current. This convective transport in essence acts as a time-

delayed negative feedback loop as the convection from the bulk of the solution depends on the electrochemical current at the surface of the electrode. Through this simple model, we can qualitatively reproduce the frequency and the magnitude of the observed oscillations (Figure 5). We did not attempt to achieve quantitative reproduction of the oscillatory behavior as that would require overparameterization of the experimental system. Rather than attempting to fit the kinetic time constants to the experimental data, we used reasonable estimates for these time constants to achieve behavior that qualitatively matches the experiments. In the future, we hope to quantitatively reproduce the oscillatory behavior through a multiscale model that captures the effects of the magnetic field on the fluid and the interaction of the fluid/mass transfer characteristics on the observed electrochemical current.

Finally, when we compared the products formed during EOG with no applied magnetic field and a 0.3 T field at 1.35 V for a 10% v/v solution of glycerol in 1 M KOH, we observed that we were able to increase the concentrations of partially oxidized species, including glyceric acid (Table 1). We

Table 1. Table Comparing the Product Selectivity for Oxidation of Glycerol at 10 wt % Glycerol and 1.35 V with a 0.0 and 0.3 T Applied Field

	product selectivity (%)	
	0.0 T	0.3 T
glyceraldehyde	17	12
glyceric acid	14	29
dihydroxyacetone	10	15
formic acid	28	23
CO	8	6
CO_2	22	14

observed up to a 2.1× increase in the yield of glyceric acid with quantitative ^{13}C NMR than the same sample with no applied magnetic field; however, glyceric acid is a minority product that accounted for up to ~14% of the oxidized glycerol in the case of no applied field (~30% in the presence of a 0.3 T field) (see the Supporting Information for details of the product characterization). Further optimization of this oscillatory system may lead to the generation of enhanced selectivity for minority products such as glyceric acid. These results were also independently reproduced by three researchers in our laboratories. We were able to consistently

quantitatively reproduce the electrochemical experiments with the RDE and magnetic fields (<20% variation in measured current). The Supporting Information contains details (Figures S11 and S12) concerning replicability/reliability of the experimental results. While we did not compare how the oscillation frequency affects the product distribution, we suspect that a change in the oscillation frequency would change the time-averaged concentrations of reactants (i.e., glycerol and glyceraldehyde) due to changes in the time-averaged fluid flow near the surface of the electrode. This relationship between the frequency of oscillations and the observed distribution of products would be hard to delineate as the frequency of oscillations depends nonlinearly on the concentration of glycerol and on the applied potential.

We believe one mechanism for these large changes in selectivity may be that the magnetic fields change the effective polarization overpotential near the surface of the electrode. Koper and Kwon showed that increasing or decreasing the applied potential by 0.2 V for EOG could decrease the selectivity for glyceric and glycolic acid by nearly a factor of 2.[47] One possible mechanism for the large changes in selectivity is that the sudden increases in mass transport due to the magnetic field decreasing the polarization overpotential near the electrode. This change in polarization overpotential could change the effective potential of the electrode and thus modified selectivity. Similarly, the concentrations of species near the electrode surface could affect the observed selectivity. In the future, we hope to perform detailed electrochemical simulations to determine the mechanism behind these large changes in selectivity.

One possible mechanism for generating oscillatory behavior could involve the magnetohydrodynamic effects interacting with themselves; this interaction would take the form of a static magnetic field increasing the mass transport and electrochemical current for an electrochemical reaction. The increase of the electrochemical current then increases the magnitude of the magnetohydrodynamic effects (as more ions begin to move in the electrochemical cell) which restarts the cycle. We do not believe that the fluid motion generated by the magnetic fields could begin to interact with itself (due to the dependence of these magnetic field effects on the current density) and lead to autocatalytic or self-inhibitory behavior occurring in our system. In our system, we do not believe a mechanism that includes feedback of the magnetohydrodynamic effects acting on themselves (through the dependence of the magneto-hydrodynamic effects on the electrochemical current, where the electrochemical current is also affected by the magneto-hydrodynamics of the electrochemical cell) is a major contributor as the oscillations are up to 24% of the current density.

CONCLUSIONS

This paper demonstrates that application of a static magnetic field during electrocatalytic oxidation of glycerol (EOG) increases mass transport through the Lorentz force. We used magnetic fields to couple mass transport generated by the Lorentz force to the electrochemical oxidation of glycerol, generating oscillatory behavior in the current density observed for the electrochemical oxidation of glycerol. We performed rotating disk electrode (RDE) experiments and particle-imaging velocimetry (PIV) measurements to show that magnetic fields increase mass transport during EOG. We showed that the Lorentz force acts on ion transport

(hydronium and hydroxide ions) during EOG to enhance mass transport by generating convection in the electrolyte. We used PIV to demonstrate that the fluid flow field generated by the magnetic fields depends nonlinearly on the viscosity of the solution (dictated by the concentration of glycerol which ranged from 2.5 to 40% to give a viscosity range of 1.3−5.3 mPa s). We used this nonlinear dependence of the fluid flow on the viscosity to generate time-delayed negative feedback during EOG by coupling the fluid flow field to the oxidative reactions. We demonstrated that we were able to generate oscillatory behavior during EOG at potentials corresponding to the crossover voltage for oxidation of glyceraldehyde to oxidation of glycerol. The convection generated by the Lorentz force acting on moving ions acts to induce nonlinear feedback and behavior during EOG by coupling the fluid flow field to the oxidative reactions, resulting in changes to the observed selectivity at a single potential in the presence of a magnetic field when compared to no magnetic field.

In future works, we hope to (i) understand and quantitatively predict the oscillation mechanism and the effects on selectivity and (ii) demonstrate potential uses of magnetic fields for fuel cells. Particularly, MHD effects should be able to decrease any energetic costs associated with pumping fluid for a glycerol-based fuel cell and could potentially shift the selectivity of the reaction toward a more desirable product distribution, increasing the techno-economics of the process.

■ ASSOCIATED CONTENT

ⓈI Supporting Information

The Supporting Information is available free of charge at https://pubs.acs.org/doi/10.1021/acs.jpcc.2c05145.

Experimental procedures, spectroscopic data (PDF)

Video S1 (MP4)

Video S2 (MP4)

Video S3 (MP4)

Video S4 (MP4)

■ AUTHOR INFORMATION

Corresponding Author

George M. Whitesides — *Department of Chemistry and Chemical Biology, Harvard University, Cambridge, Massachusetts 02138, United States;* ⓞ orcid.org/0000-0001-9451-2442; Email: gwhitesides@gmwgroup.harvard.edu

Authors

Rui Gao — *Department of Chemistry and Chemical Biology, Harvard University, Cambridge, Massachusetts 02138, United States*

Mohamad S. Kodaimati — *Department of Chemistry and Chemical Biology, Harvard University, Cambridge, Massachusetts 02138, United States*

Kaitlyn M. Handy — *Department of Chemistry and Chemical Biology, Harvard University, Cambridge, Massachusetts 02138, United States*

Samuel E. Root — *Department of Chemistry and Chemical Biology, Harvard University, Cambridge, Massachusetts 02138, United States*

Complete contact information is available at:
https://pubs.acs.org/10.1021/acs.jpcc.2c05145

Author Contributions

M.S.K. and R.G. contributed equally to this work. M.S.K., R.G., and G.M.W. conceived of the project. M.S.K., R.G., K.M.H., and S.E.R. performed the experiments. All authors wrote the paper.

Notes

The authors declare no competing financial interest.

■ REFERENCES

(1) Xing, F.; Nakaya, Y.; Yasumura, S.; Shimizu, K.; Furukawa, S. Ternary Platinum-Cobalt-Indium Nanoalloy on Ceria as a Highly Efficient Catalyst for the Oxidative Dehydrogenation of Propane Using CO$_2$. Nat. Catal. 2022, 5, 55−65.

(2) Shen, T.-H.; Spillane, L.; Peng, J.; Shao-Horn, Y.; Tileli, V. Switchable Wetting of Oxygen-Evolving Oxide Catalysts. Nat. Catal. 2022, 5, 30−36.

(3) Liu, Y.; Qiu, H.; Li, J.; Guo, L.; Ager, J. W. Tandem Electrocatalytic CO$_2$ Reduction with Efficient Intermediate Conversion over Pyramid-Textured Cu-Ag Catalysts. ACS Appl. Mater. Interfaces 2021, 13, 40513−40521.

(4) Nam, D.-H.; De Luna, P.; Rosas-Hernández, A.; Thevenon, A.; Li, F.; Agapie, T.; Peters, J. C.; Shekhah, O.; Eddaoudi, M.; Sargent, E. H. Molecular Enhancement of Heterogeneous CO$_2$ Reduction. Nat. Mater. 2020, 19, 266−276.

(5) De Luna, P.; Liang, W.; Mallick, A.; Shekhah, O.; García de Arquer, F. P.; Proppe, A. H.; Todorović, P.; Kelley, S. O.; Sargent, E. H.; Eddaoudi, M. Metal-Organic Framework Thin Films on High-Curvature Nanostructures toward Tandem Electrocatalysis. ACS Appl. Mater. Interfaces 2018, 10, 31225−31232.

(6) Chen, C.; Li, Y.; Yu, S.; Louisia, S.; Jin, J.; Li, M.; Ross, M. B.; Yang, P. Cu-Ag Tandem Catalysts for High-Rate CO$_2$ Electrolysis toward Multicarbons. Joule 2020, 4, 1688−1699.

(7) Xie, C.; Chen, C.; Yu, Y.; Su, J.; Li, Y.; Somorjai, G. A.; Yang, P. Tandem Catalysis for CO$_2$ Hydrogenation to C2-C4 Hydrocarbons. Nano Lett. 2017, 17, 3798−3802.

(8) Duncan, T. M.; Reimer, J. A. Chemical Engineering Design and Analysis. Chemical Engineering Design and Analysis. 2019.

(9) Wang, M.; Na, Y.; Gorlov, M.; Sun, L. Light-Driven Hydrogen Production Catalysed by Transition Metal Complexes in Homogeneous Systems. Dalt. Trans. 2009, 33, 6458−6467.

(10) Chang, K.; Hai, X.; Ye, J. Transition Metal Disulfides as Noble-Metal-Alternative Co-Catalysts for Solar Hydrogen Production. Adv. Energy Mater. 2016, 6, 1502555.

(11) Rodríguez-Lugo, R. E.; Trincado, M.; Vogt, M.; Tewes, F.; Santiso-Quinones, G.; Grützmacher, H. A Homogeneous Transition Metal Complex for Clean Hydrogen Production from Methanol-Water Mixtures. Nat. Chem. 2013, 5, 342−347.

(12) Wang, J.; Zhang, H.; Wang, X. Recent Methods for the Synthesis of Noble-Metal-Free Hydrogen-Evolution Electrocatalysts: From Nanoscale to Sub-nanoscale. Small Methods 2017, 1, 1700118.

(13) Beyene, B. B.; Hung, C.-H. Recent Progress on Metalloporphyrin-Based Hydrogen Evolution Catalysis. Coord. Chem. Rev. 2020, 410, 213234.

(14) Faulkner, A.; van Leeuwen, T.; Feringa, B. L.; Wezenberg, S. J. Allosteric Regulation of the Rotational Speed in a Light-Driven Molecular Motor. J. Am. Chem. Soc. 2016, 138, 13597−13603.

(15) Strazewski, P. The Essence of Systems Chemistry. Life 2019, 9, 60.

(16) Mattia, E.; Otto, S. Supramolecular Systems Chemistry. Nat. Nanotechnol. 2015, 10, 111−119.

(17) Gibb, B. C. Teetering towards Chaos and Complexity. Nat. Chem. 2009, 1, 17−18.

(18) Nitschke, J. R. Molecular Networks Come of Age. Nature 2009, 462, 736−738.

(19) Whitesides, G. M.; Ismagilov, R. F. Complexity in Chemistry. Science 1999, 284, 89−92.

(20) Miljanić, O. Š. Small-Molecule Systems Chemistry. Chem. 2017, 2, 502−524.

(21) Epstein, I. R.; Xu, B. Reaction-Diffusion Processes at the Nano- and Microscales. Nat. Nanotechnol. 2016, 11, 312−319.

(22) Vanag, V. K.; Epstein, I. R. Segmented Spiral Waves in a Reaction-Diffusion System. Proc. Natl. Acad. Sci. U. S. A. 2003, 100, 14635−14638.

(23) Semenov, S. N.; Kraft, L. J.; Ainla, A.; Zhao, M.; Baghbanzadeh, M.; Campbell, V. E.; Kang, K.; Fox, J. M.; Whitesides, G. M. Autocatalytic, Bistable, Oscillatory Networks of Biologically Relevant Organic Reactions. Nature 2016, 537, 656−660.

(24) Cafferty, B. J.; Wong, A. S. Y.; Semenov, S. N.; Belding, L.; Gmur, S.; Huck, W. T. S.; Whitesides, G. M. Robustness, Entrainment, and Hybridization in Dissipative Molecular Networks, and the Origin of Life. J. Am. Chem. Soc. 2019, 141, 8289−8295.

(25) Kurin-Csörgei, K.; Epstein, I. R.; Orbán, M. Systematic Design of Chemical Oscillators Using Complexation and Precipitation Equilibria. Nature 2005, 433, 139−142.

(26) Ciriminna, R.; Pina, C. D.; Rossi, M.; Pagliaro, M. Understanding the Glycerol Market. Eur. J. Lipid Sci. Technol. 2014, 116, 1432−1439.

(27) Anitha, M.; Kamarudin, S. K.; Kofli, N. T. The Potential of Glycerol as a Value-Added Commodity. Chem. Eng. J. 2016, 295, 119−130.

(28) Quispe, C. A. G.; Coronado, C. J. R.; Carvalho, J. A. Glycerol: Production, Consumption, Prices, Characterization and New Trends in Combustion. Renew. Sustain. Energy Rev. 2013, 27, 475−493.

(29) Bianchini, C.; Shen, P. K. Palladium-Based Electrocatalysts for Alcohol Oxidation in Half Cells and in Direct Alcohol Fuel Cells. Chem. Rev. 2009, 109, 4183−4206.

(30) Antolini, E. Glycerol Electro-Oxidation in Alkaline Media and Alkaline Direct Glycerol Fuel Cells. Catal. 2019, 9, 980.

(31) Marchionni, A.; Bevilacqua, M.; Bianchini, C.; Chen, Y. X.; Filippi, J.; Fornasiero, P.; Lavacchi, A.; Miller, H.; Wang, L.; Vizza, F. Electrooxidation of Ethylene Glycol and Glycerol on Pd-(Ni-Zn)/C Anodes in Direct Alcohol Fuel Cells. ChemSusChem 2013, 6, 518−528.

(32) Zakaria, K.; McKay, M.; Thimmappa, R.; Hasan, M.; Mamlouk, M.; Scott, K. Direct Glycerol Fuel Cells: Comparison with Direct Methanol and Ethanol Fuel Cells. ChemElectroChem 2019, 6, 2578−2585.

(33) Haynes, W. M.CRC Handbook of Chemistry and Physics; CRC Press: 2014.

(34) Verma, S.; Lu, S.; Kenis, P. J. A. Co-Electrolysis of CO$_2$ and Glycerol as a Pathway to Carbon Chemicals with Improved Technoeconomics Due to Low Electricity Consumption. Nat. Energy 2019, 4, 466−474.

(35) Yadegari, H.; Ozden, A.; Alkayyali, T.; Soni, V.; Thevenon, A.; Rosas-Hernández, A.; Agapie, T.; Peters, J. C.; Sargent, E. H.; Sinton, D. Glycerol Oxidation Pairs with Carbon Monoxide Reduction for Low-Voltage Generation of C2 and C3 Product Streams. ACS Energy Lett. 2021, 6, 3538−3544.

(36) Na, J.; Seo, B.; Kim, J.; Lee, C. W.; Lee, H.; Hwang, Y. J.; Min, B. K.; Lee, D. K.; Oh, H.-S.; Lee, U. General Technoeconomic Analysis for Electrochemical Coproduction Coupling Carbon Dioxide Reduction with Organic Oxidation. Nat. Commun. 2019, 10, 1−13.

(37) Kwon, Y. C. S.; Lai, S.; Rodriguez, P. T. M.; Koper, M. Electrocatalytic Oxidation of Alcohols on Gold in Alkaline Media: Base or Gold Catalysis? *J. Am. Chem. Soc.* **2011**, *133*, 6914−6917.

(38) Schell, M.; Xu, Y.; Zdraveski, Z. Mechanism for the Electrocatalyzed Oxidation of Glycerol Deduced from an Analysis of Chemical Instabilities. *J. Phys. Chem.* **1996**, *100*, 18962−18969.

(39) Oliveira, C. P.; Lussari, N. V.; Sitta, E.; Varela, H. Oscillatory Electro-Oxidation of Glycerol on Platinum. *Electrochim. Acta* **2012**, *85*, 674−679.

(40) Melle, G.; de Souza, M. B. C.; Santiago, P. V. B.; Corradini, P. G.; Mascaro, L. H.; Fernández, P. S.; Sitta, E. Glycerol Electro-Oxidation at Pt in Alkaline Media: Influence of Mass Transport and Cations. *Electrochim. Acta* **2021**, *398*, 139318.

(41) Melle, G. B.; Machado, E. G.; Mascaro, L. H.; Sitta, E. Eff Ect of Mass Transport on the Glycerol Electro-Oxidation. *Electrochim. Acta* **2019**, *296*, 972−979.

(42) Kwon, Y.; Birdja, Y.; Spanos, I.; Rodriguez, P.; Koper, M. T. M. Highly Selective Electro-Oxidation of Glycerol to Dihydroxyacetone on Platinum in the Presence of Bismuth. *ACS Catal.* **2012**, *2*, 759−764.

(43) Zhou, Y.; Shen, Y.; Xi, J.; Luo, X. Selective Electro-Oxidation of Glycerol to Dihydroxyacetone by PtAg Skeletons. *ACS Appl. Mater. Interfaces* **2019**, *11*, 28953−28959.

(44) Garcia, A. C.; Kolb, M. J.; Van Nierop Y Sanchez, C.; Vos, J.; Birdja, Y. Y.; Kwon, Y.; Tremiliosi-Filho, G.; Koper, M. T. M. Strong Impact of Platinum Surface Structure on Primary and Secondary Alcohol Oxidation during Electro-Oxidation of Glycerol. *ACS Catal.* **2016**, *6*, 4491−4500.

(45) Hu, W.; Lowry, B.; Varma, A. Kinetic Study of Glycerol Oxidation Network over Pt-Bi/C Catalyst. *Appl. Catal. B Environ.* **2011**, *106*, 123−132.

(46) Kwon, Y.; Lai, S. C. S.; Rodriguez, P.; Koper, M. T. M. Electrocatalytic Oxidation of Alcohols on Gold in Alkaline Media: Base or Gold Catalysis? *J. Am. Chem. Soc.* **2011**, *133*, 6914−6917.

(47) Kwon, Y.; Koper, M. T. M. Combining Voltammetry with HPLC: Application to Electro-Oxidation of Glycerol. *Anal. Chem.* **2010**, *82*, 5420−5424.

(48) Gomes, J. F.; De Paula, F. B. C.; Gasparotto, L. H. S.; Tremiliosi-Filho, G. The Influence of the Pt Crystalline Surface Orientation on the Glycerol Electro-Oxidation in Acidic Media. *Electrochim. Acta* **2012**, *76*, 88−93.

(49) Zhou, J.; Hu, J.; Zhang, X.; Li, J.; Jiang, K.; Liu, Y.; Zhao, G.; Wang, X.; Chu, H. Facet Effect of Pt Nanocrystals on Catalytical Properties toward Glycerol Oxidation Reaction. *J. Catal.* **2020**, *381*, 434−442.

(50) Gomes, J. F.; Tremiliosi-Filho, G. Spectroscopic Studies of the Glycerol Electro-Oxidation on Polycrystalline Au and Pt Surfaces in Acidic and Alkaline Media. *Electrocatalysis* **2011**, *2*, 96−105.

(51) Kodaimati, M. S.; Gao, R.; Root, S. E.; Whitesides, G. M. Magnetic Fields Enhance Mass Transport during Electrocatalytic Reduction of CO_2. *Chem. Catal.* **2022**, *2*, 797−815.

(52) Lioubashevski, O.; Katz, E.; Willner, I. Magnetic Field Effects on Electrochemical Processes: A Theoretical Hydrodynamic Model. *J. Phys. Chem. B* **2004**, *108*, 5778−5784.

(53) Hinds, G.; Spada, F. E.; Coey, J. M. D.; Ní; Mhíocháin, T. R.; Lyons, M. E. G. Magnetic Field Effects on Copper Electrolysis. *J. Phys. Chem. B* **2001**, *105*, 9487−9502.

(54) Ragsdale, S. R.; Grant, K. M.; White, H. S. Electrochemically Generated Magnetic Forces. Enhanced Transport of a Paramagnetic Redox Species in Large, Nonuniform Magnetic Fields. *J. Am. Chem. Soc.* **1998**, *120*, 13461−13468.

(55) Bhargava, S. S.; Azmoodeh, D.; Chen, X.; Cofell, E. R.; Esposito, A. M.; Verma, S.; Gewirth, A. A.; Kenis, P. J. A. Decreasing the Energy Consumption of the CO_2 Electrolysis Process Using a Magnetic Field. *ACS Energy Lett.* **2021**, *6*, 2427−2433.

(56) Li, Y.-H.; Chen, Y.-J. The Effect of Magnetic Field on the Dynamics of Gas Bubbles in Water Electrolysis. *Sci. Rep.* **2021**, *11*, 9346.

(57) Yu, Q.-K.; Miyakita, Y.; Nakabayashi, S.; Baba, R. Magnetic Field Effect on Electrochemical Oscillations during Iron Dissolution. *Electrochem. Commun.* **2003**, *S*, 321−324.

(58) Marinaro, G.; Huang, M.; Mutschke, G.; Yang, X.; Eckert, K. Oscillatory Copper Deposition on Conical Iron Electrodes in a Nonuniform Magnetic Field. *Magnetochemistry* **2021**, *7*, 46.

(59) Lioubashevski, O.; Katz, E.; Willner, I. Effects of Magnetic Field Directed Orthogonally to Surfaces on Electrochemical Processes. *J. Phys. Chem. C* **2007**, *111*, 6024−6032.

(60) Monzon, L. M. A.; Coey, J. M. D. Magnetic Fields in Electrochemistry: The Lorentz Force. A Mini-Review. *Electrochem. Commun.* **2014**, *42*, 38−41.

(61) Kubo, R. The Fluctuation-Dissipation Theorem. *Rep. Prog. Phys.* **1966**, *29*, 255−284.

(62) Raffel, M.; Willert, C. E.; Scarano, F.; Kähler, C. J.; Wereley, S. T.; Kompenhans, J.*Particle Image Velocimetry: A Practical Guide*; Springer: 2018.

(63) Thielicke, W.; Stamhuis, E. PIVlab@ Towards User-Friendly, Affordable and Accurate Digital Particle Image Velocimetry in MATLAB. *J. open Res. Softw.* **2014**, *2*, 30.

(64) Feynman, R. P.*Feynman Lectures on Physics. Volume 2: Mainly Electromagnetism and Matter*, 1964.

(65) Novák, B.; Tyson, J. J. Design Principles of Biochemical Oscillators. *Nat. Rev. Mol. Cell Biol.* **2008**, *9*, 981−991.